REPORT DOCUMENTATION PAGE

Form Approved
OMB No. 0704-0188

1. REPORT DATE *(DD-MM-YYYY)*	**2. REPORT TYPE**	**3. DATES COVERED** *(From - To)*
01-05-2006	Conference Paper POSTPRINT	2005 - 2006

4. TITLE AND SUBTITLE
Development of Deployable Elastic Composite Shape Memory Alloy Reinforced (DECSMAR) Structures

5a. CONTRACT NUMBER
FA9453-05-C-0005

5b. GRANT NUMBER

5c. PROGRAM ELEMENT NUMBER
63401F

6. AUTHOR(S)
Eric L. Pollard and Thomas W. Murphey*

5d. PROJECT NUMBER
682J

5e. TASK NUMBER
SY

5f. WORK UNIT NUMBER
0A

7. PERFORMING ORGANIZATION NAME(S) AND ADDRESS(ES) AND ADDRESS(ES)
CSA Engineering, Inc.
1451 Innovation Pkwy SE, Suite 100
Albuquerque, NM 87123-3831

8. PERFORMING ORGANIZATION REPORT NUMBER

9. SPONSORING / MONITORING AGENCY NAME(S) AND ADDRESS(ES)
*Air Force Research Laboratory
Space Vehicles
3550 Aberdeen Ave SE
Kirtland AFB, NM 87117-5776

10. SPONSOR/MONITOR'S ACRONYM(S)

11. SPONSOR/MONITOR'S REPORT NUMBER(S)
AFRL-VS-PS-TP-2006-1019

12. DISTRIBUTION / AVAILABILITY STATEMENT

Approved for public release; distribution is unlimited. (Clearance #VS06-0106)

13. SUPPLEMENTARY NOTES
Published in the 47th AIAA/ASME/ASCE/AHS/ASC Structures, Structural Dynamics, and Materials Conference Proceedings, 1 – 4 May 2006, Newport, RI, AIAA 2006-1681.

14. ABSTRACT
The objective of this research is to develop a novel. self-deployable truss architecture composed of carbon fiber reinforced plastic (CFRP) tape-spring elements and embedded shape memory alloy (SMA) flexures; this particular structural system is referred to as deployable elastic composite shape memory alloy reinforced (DECSMAR) and is representative of a concentrated, material deformation based deployable architecture. The scope of this study encompasses applying fundamental principles of rational boom design relevant to all deployable structures, first to define the design space of the individual CFRP tape-spring element, then to conduct an exercise for a point design of a 180 mm radius DECSMAR boom with correlation to experimental analysis, and finally to explore performance implications of scaling the truss radius. Of particular interest was the design of the CFRP tape-spring element elastic-stability and stiffness properties, then to understand how load-path allocation between the frame-like longerons and battens and tension only diagonals proportions energy imparted from global loading through the structural network; thermal response was not investigated. Characterizing the enhancement the SMA flexure features purchase and design issues for package envelop optimization are pertinent to both individual CFRP tape-spring element and system wide design and are discussed throughout. Aspects of the architecture for tackle to further develop DECSMAR, including the self-deployment scheme, will be focused on in a sequel manuscript to appear. Technology addressed through this research is intended to foster and mature successive large, launch-packaged concentrated strain structures.

15. SUBJECT TERMS
Self-Deployable Truss Architecture, Carbon Fiber Reinforced Plastic, CFRP, Tape Spring, DECSMAR, Rational Boom Design

16. SECURITY CLASSIFICATION OF:			**17. LIMITATION OF ABSTRACT**	**18. NUMBER OF PAGES**	**19a. NAME OF RESPONSIBLE PERSON**
a. REPORT	**b. ABSTRACT**	**c. THIS PAGE**			Thomas W. Murphey
Unclassified	Unclassified	Unclassified	Unlimited	19	**19b. TELEPHONE NUMBER** *(include area code)* 505-846-9969

47th AIAA/ASME/ASCE/AHS/ASC Structures, Structural Dynamics, and Materials Conference<BR
1 - 4 May 2006, Newport, Rhode Island

AIAA 2006-1681

Development of Deployable Elastic Composite Shape Memory Alloy Reinforced (DECSMAR) Structures

Eric L Pollard*
CSA Engineering, Inc., Albuquerque, NM 87123-3831 US

&
Thomas W Murphey†
Air Force Research Laboratory, Albuquerque, NM, 87117-5776 US

The objective of this research is to develop a novel. self-deployable truss architecture composed of carbon fiber reinforced plastic (CFRP) tape-spring elements and embedded shape memory alloy (SMA) flexures; this particular structural system is referred to as deployable elastic composite shape memory alloy reinforced (DECSMAR) and is representative of a concentrated, material deformation based deployable architecture. The scope of this study encompasses applying fundamental principles of rational boom design relevant to all deployable structures, first to define the design space of the individual CFRP tape-spring element, then to conduct an exercise for a point design of a 180 mm radius DECSMAR boom with correlation to experimental analysis, and finally to explore performance implications of scaling the truss radius. Of particular interest was the design of the CFRP tape-spring element elastic-stability and stiffness properties, then to understand how load-path allocation between the frame-like longerons and battens and tension only diagonals proportions energy imparted from global loading through the structural network; thermal response was not investigated. Characterizing the enhancement the SMA flexure features purchase and design issues for package envelop optimization are pertinent to both individual CFRP tape-spring element and system wide design and are discussed throughout. Aspects of the architecture for tackle to further develop DECSMAR, including the self-deployment scheme, will be focused on in a sequel manuscript to appear. Technology addressed through this research is intended to foster and mature successive large, launch-packaged concentrated strain structures.

Nomenclature

A	=	area
E	=	modulus of elasticity
G	=	shear modulus of elasticity
h	=	thickness
I	=	area moment of inertia
l	=	element length
L	=	truss length
m	=	mass
M	=	moment
n	=	number of longerons
P	=	load
R	=	radius
u	=	performance index
V	=	shear load

* Engineer, CSA Engineering, Inc., 1451 Innovation Pkwy. SE Suite 100, Albuquerque, NM 87123-3831 US, AIAA Young Professional Member
† Research Aerospace Engineer, Space Vehicles Directorate, 3550 Aberdeen Ave. SE, Albuquerque, NM 87117-5776 US, AIAA Professional Member

w = linear mass
θ = diagonal angle
v = Poisson's ratio
φ = subtended angle

$_{b}$ = batten
$_{bend}$ = bending
$_{d}$ = diagonal
$_{e}$ = element
$_{l}$ = longeron
$_{ls}$ = linear specific

I. Introduction

COMPOSITE systems of carbon fiber reinforced plastic (CFRP) have historically served stiff, non-compliant structural applications, taking advantage of the competitive mass density of these materials relative to metallic systems.[1] Yet, architectures composed of reasonably thin laminate elements with geometric stiffness, i.e. tape-springs, can utilize composite high-strength properties and yield a compliant structure relevant to deployable space applications.[2] Monolithic systems packaged through concentrated, material deformation at discrete hinge regions have no dead-band and can exploit stored strain energy to motivate self-deployment. Shape memory alloy (SMA), capable of superelasticity, feature additions have been found to compliment composite hinges. Since discovery, superelasticity, a recoverable, solid-phase dependent inelastic deformation mechanism, has been identified as a potential agency to drive active material systems.[3] SMAs are particularly attractive for space applications due to their ability to recover large deformations by generating high specific force, resulting artifacts of the mechanically induced austenite-martensite crystalline phase transformation. Deployment and in-service challenges of large, launch-packaged space vehicle programs is expected to showcase the leverage SMA reinforced high-strength composite technology extends to structural reconfiguration and performance tailoring.

A. Concept

The deployable elastic composite shape memory alloy reinforced (DECSMAR) truss concept is a novel, self-deployable truss architecture composed of CFRP tape-spring elements and embedded SMA flexures (Fig. 1). The non-prismatic longerons have traverse reduced thickness gauge sections to enable equal and opposite bending where the length of the reduced thickness regions corresponds to the radius of the fold and pi; consequently the thickness and length of the hinge region or the distance from the neutral-plane and the bend radius dictate the strain realized. In order to minimize the bend radius for increased compaction efficiency, a less structurally efficient material system is utilized for the hinge regions while a more efficient and less compliant material system is utilized throughout the majority of the structure. It may not be intuitive this pairing of structural roles leads to greater mass efficiency as well. These monolithic hinges are deliberately placed to enforce packaging kinematics; longerons z-fold and the battens nest. To mitigate the compromise of deployed performance due to the hinge cross-section, Nitinol SMA wires can be embedded in the composite lay-up across the reduced thickness region, thicker wires of binary NiTi can accommodate the same radius as the thinner CRFP through superelastic deformation.

(a) **(b)**

Fig. 1 Three-bay DECSMAR truss prototype, (a) stowed configuration; (b) deployed architecture

B. Background

Deployable structures are typically implemented by one of two approaches. Most commonly, deployment is accommodated through rolling or sliding contact joint mechanisms. These articulated structures employ mechanical components such as pin-clevis joints, ball and socket joints, and Rolamite joints and are characteristic of commercial products such as the AEC-ABLE Adam boom and PUMA solar arrays.[4] The second approach is to use material deformations to accommodate folding. Heritage examples of this approach are coilable longeron masts such as AEC-ABLE and NG Astro, TRW spring-back reflectors, wrap rib reflectors, and STEMs. Recently, there has been renewed interest in the development of deployable structure architectures based on material deformations. The majority of these efforts have focused on the development of CFRP material systems that employ a softened resin state to accommodate large deformations and a stiffer rigidized state after deployment. More recently, there has been renewed interest in material deformation based architectures that do not rely on resin softening. These architectures employ traditional resin systems that behave elastically during and after deployment. Examples of this approach are Foster-Miller hinges, Astro Flat Folding Tube, and the Alan Wat reflector. In these elastic material deformation approaches, a single material system of constant thickness is used throughout the structure, whether or not it needs to fold.

C. Objective

The objective of this research is to develop the DECSMAR truss concept, an example of a concentrated, material deformation approach to deployable architectures. The scope of this study encompasses applying fundamental principles of rational boom design relevant to all deployable structures, first to define the design space of the individual CFRP tape-spring element, then to conduct an exercise for a point design of a 180 mm radius DECSMAR boom with correlation to experimental analysis, and finally to explore performance implications of scaling the truss radius. Of particular interest was the design of the CFRP tape-spring element elastic-stability and stiffness properties, then to understand how load-path allocation between the frame-like longerons and battens and tension only diagonals proportions energy imparted from global loading through the structural network; thermal response was not investigated. Characterizing the enhancement the SMA flexure features purchase and design issues for

package envelop optimization are pertinent to both individual CFRP tape-spring element and system wide design and are discussed throughout.

II. Design Space of CFRP Tape-Spring Element

A numerical and analytical study of the CFRP tape-spring element elastic-stability and stiffness properties has been conducted for parametrically varying material system, laminate thickness, radius, and subtended angle to understand the trades between these parameters (Fig. 2). These attributes influence the deployed truss's strength and stiffness performance and design of the SMA reinforced hinge sections, driving the packaged envelope. The length of the model evaluated on both critical axial load and the cross-section axial modulus is unique to the repetitive longeron element traceable to the point design at 170 mm. The ABAQUS Standard finite element code's subspace eigensolver was employed to solve for the buckling loads and modes.[5] Mesh refinement convergence was sought for the first negative pivot and agreement with stability solutions derived by Timoshenko.[6] Full-integration shell elements assumed to have linear moment-bending and force-membrane strain relationships assigned with composite section definitions represented the laminate models and lamina material constants were consistent with experimental results of the IM7/977-2 system.[7]

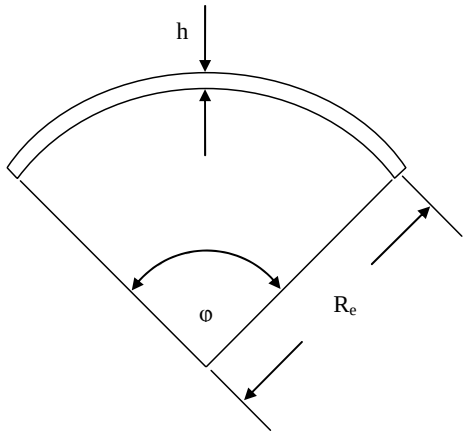

Fig. 2 Laminate thickness, radius, and subtended angle were parametrically varied to understand the trades between these parameters.

The model considered for calibration of the numerical buckling load prediction approach can be characterized as one composed of an isotropic material with E=173 GPa and ν=0.34, 254 μm thickness, subtending an angle of 120˚, and a radius of 28.6 mm; this thickness is a reasonable minimum for a cured multi-lamina sequence including both uni-directional and woven fiber prepreg to the fiber area weight limit of current manufacturing technology. The model was simply supported along all edges consistent with Timoshenko's solution for axial compression of curved sheet panels. The mesh was progressively h refined until a global seed size of 2.00 mm when the convergence of the first eigenvalue was within 18% and agreement with the Timoshenko solution was within 7% at a value of 15,392 N (Fig 3).

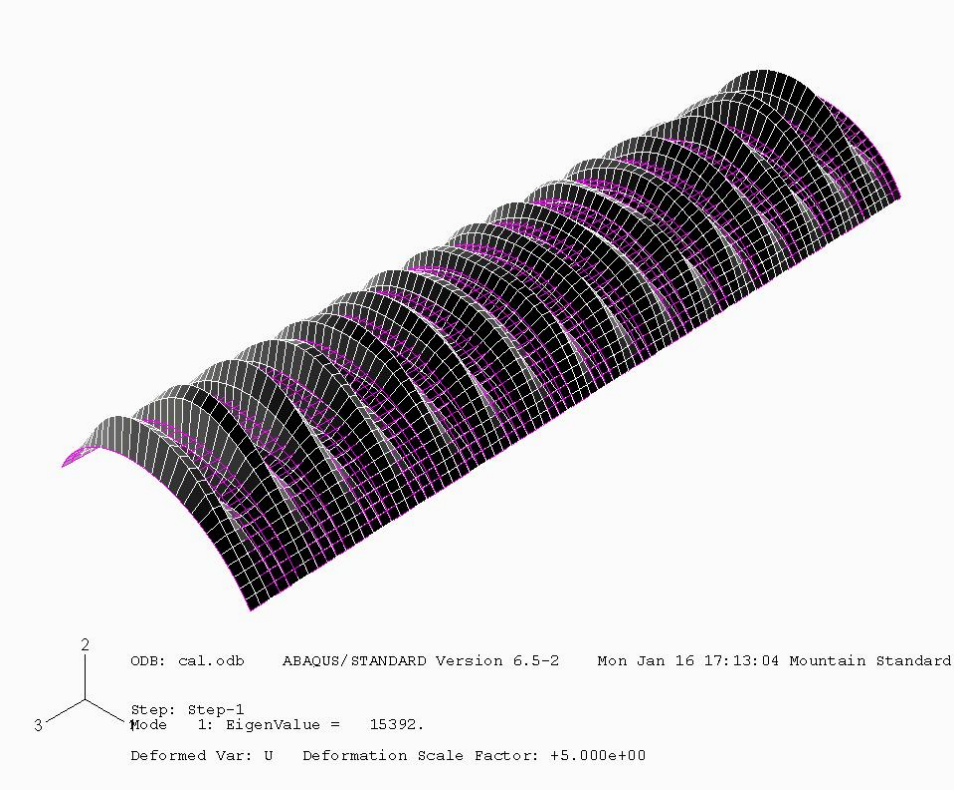

Fig. 3 First mode of calibration model for numerical buckling load prediction approach characterized as one composed of an isotropic material with *E*=173 GPa and *ν*=0.34, 254 μm thickness, subtending an angle of 120˚, and a radius of 28.6 mm, simply supported on along all edges, and progressively h refined until a global seed size of 2.00 mm at a value of 15,392 N

In order to map the design space for the proportion of off-axis fiber to serve a strength function to the sandwiched 0° material composing the CRFP tape-spring model, a metric was adopted accounting for elastic-stability and stiffness, as well as linear mass. This element performance index for bending loading of a longeron, proposed by Murphey,[8] is the product of an architecture and material index (Eq. 1).

$$u_{l,bend}u_{m,bend} = \frac{P_l^{\frac{2}{5}}\left(E_l A\right)^{\frac{1}{5}} l_l^{\frac{9}{5}}}{\pi^{\frac{4}{5}} m_l} \tag{1}$$

Plotting this index the relative merit of varying off-axis lay-up scenarios can be evaluated. Two-dimensional trends were developed for constant linear mass and varying the proportion of $\pm 45^{\circ}$ and 90° fiber to the sandwiched 0° material; all models have a laminate thickness of 254 μm as the calibration configuration as well as share radius and subtended angle parameters (Fig. 4). The numerical simulations contributing to this evaluation differed from those considered for calibration and more represented a longeron segment freed from the truss with encastre boundaries at each cross-section face and free conditions along the longitudinal edges; continuum shell stiffness properties were found based on classical lamination theory.

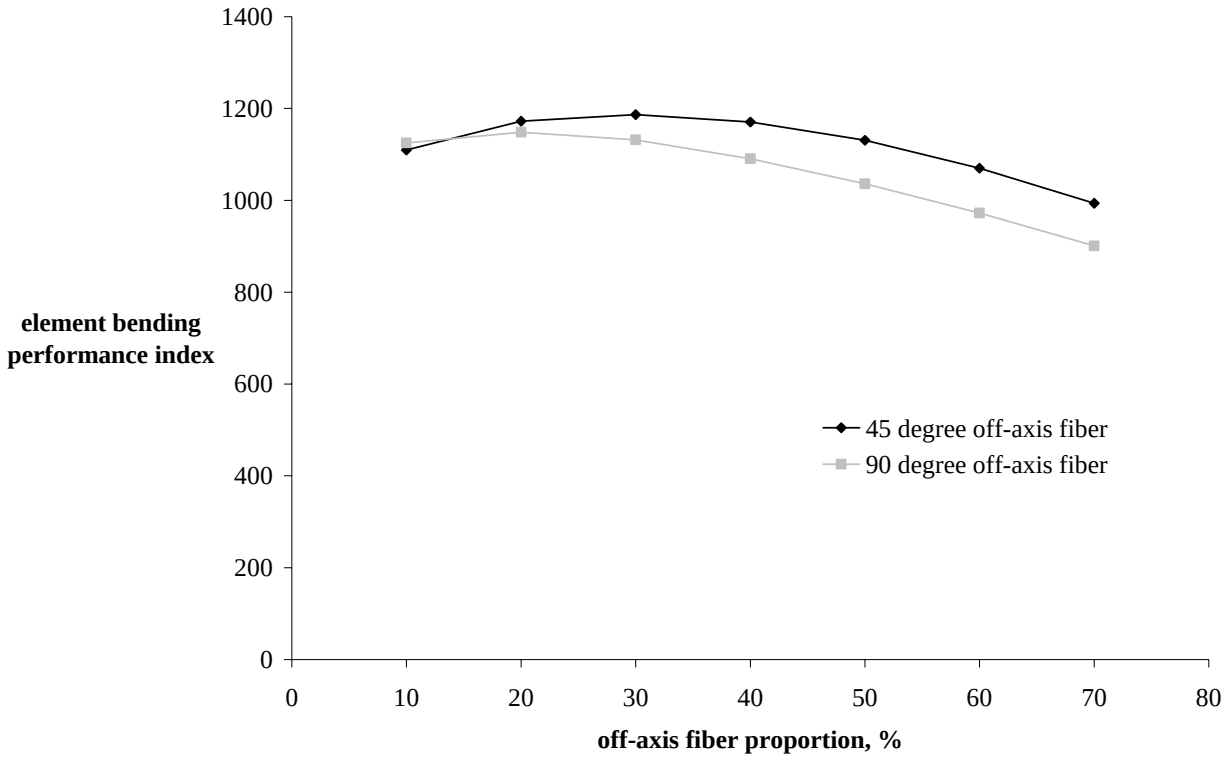

Fig. 4 Two-dimensional trends can be developed for fixed linear mass and varying the proportion of ±45° and 90° fiber to the sandwiched 0° material.

The higher qualifying candidate from Fig. 4, 30% material at ±45° plain-weave variant, was characterized at 1,187; this parameter set was identified as a reference for the remainder of the manuscript (Table 1). For perspective, a thin-walled circular cross-section element with equivalent composite lay-up sequence and linear mass scores a metric of 3,351. Consequences of varying laminate thickness and subtended angle parameters, coupled by assigning radius as a control to fix linear mass, were then investigated. Thickness was increased as, conversely, subtended angle was decreased and vice versa from the leading material system candidate; understandably, laminates thinner than 254 μm are unreasonable, but the trend is of interest (Fig. 5).

Table 1 Reference laminate

Material	Thickness	Orientation
IM7/977-2	38.1 μm	±45°
IM7/977-2	178 μm	0°
IM7/977-2	38.1 μm	±45°

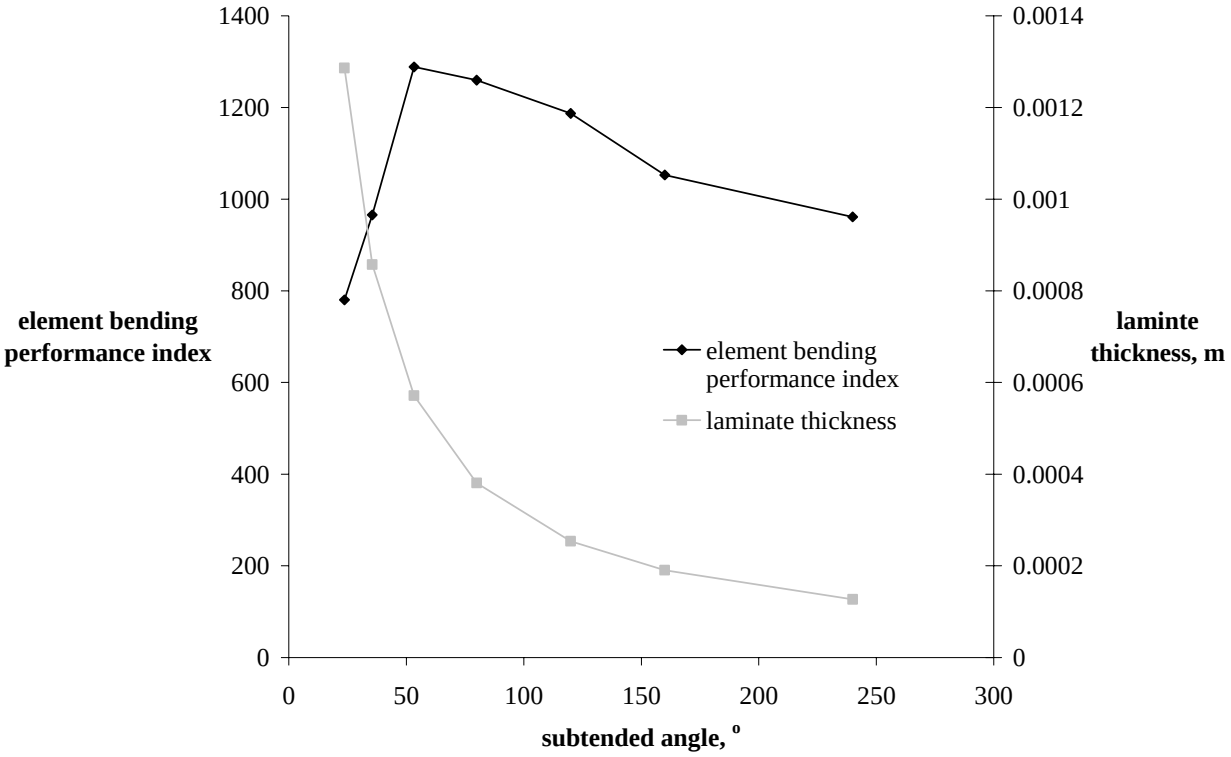

Fig. 5 Consequences of varying laminate thickness and subtended angle parameters, coupled to maintain both constant linear mass and radius, were than investigated, thickness was increased as, conversely, subtended angle was decreased and vice versa from the leading material system candidate of Fig. 4.

Strength can be gained through greater laminate thickness at angles to approximately 50˚, beyond, diminishing geometric stiffness dominates; although, another trend must be considered. For a particular allowable fiber strain, hinge radius and compaction ratio increase proportionally with laminate thickness. Consider the packaging efficiency penalty for decreasing subtended angle from 120˚ to 53˚, an increase in linear compaction ratio by a factor of 2.25. In a similar manner, consequences of varying laminate thickness and radius parameters, coupled by assigning subtended angle as a control to fix linear mass, were also investigated. Thickness was ranged inverse to radius from the leading material system candidate; again, laminates thinner than 254 μm are unreasonable, but the trend is of interest (Fig. 6).

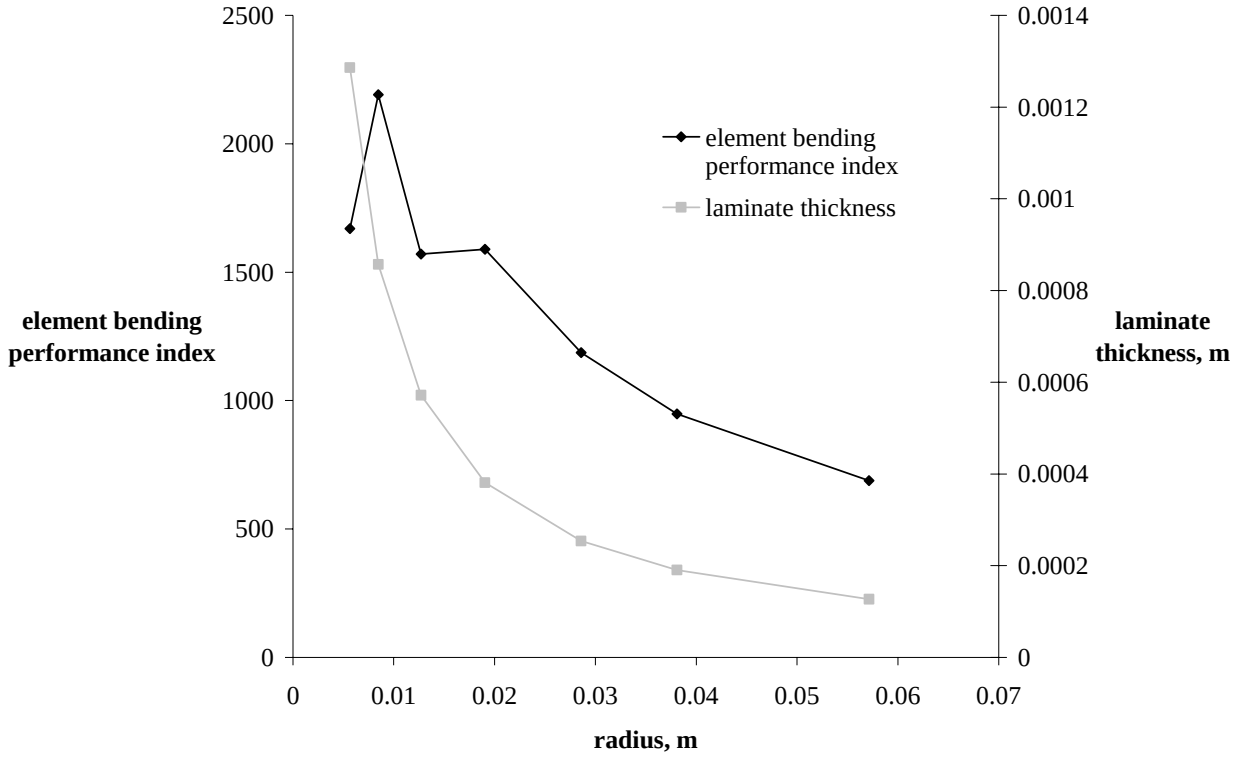

Fig. 6 Consequences of varying laminate thickness and radius parameters, coupled by assigning subtended angle as a control to fix linear mass, were also investigated. Thickness was ranged as inversely to radius from the leading material system candidate of Fig. 4.

Radius and subtended angle were traded about the 254 μm thickness, subtending an angle of 120˚, and a radius of 28.6 mm configuration with 30% material at ±45˚, now with thickness as the control to maintain constant linear mass (Fig. 7).

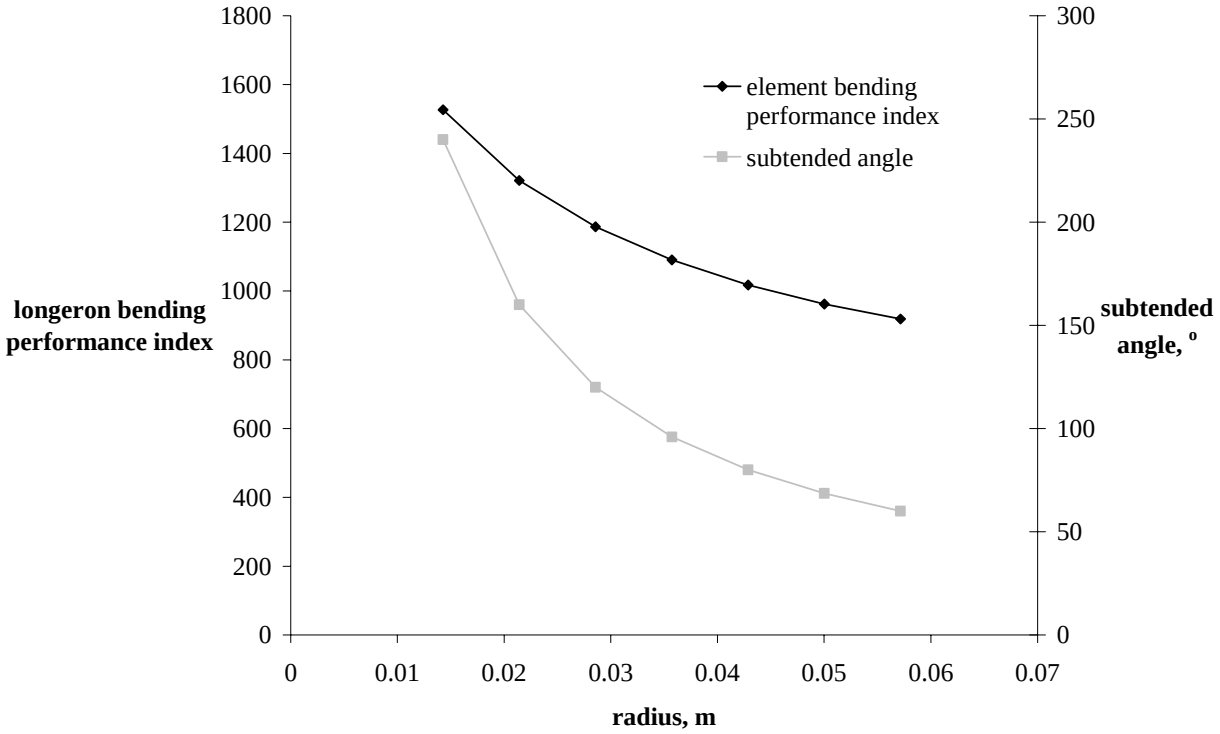

Fig. 7 Radius and subtended angle were traded about the 254 μm thickness, subtending an angle of 120˚, and a radius of 28.6 mm configuration with 30% material at ±45˚, now with thickness as the control to maintain constant linear mass.

Qualitatively, optimal CFRP tape-spring element designs can subtend angles up to 80˚ or have a radius up to 19.1 mm for a given packaging efficiency based on the trends presented in Figs. 5-6 representing 22.0 gm^{-1} linear mass. Figure 7 suggests increased performance can be achieved by decreasing radius and increasing subtended angle, but cross-sections greater than 180˚ may not be reasonable to serve kinematically as a monolithic hinge.

With some understanding of the trades for a prismatic element the features of the hinge were incorporated into the reference model by removing the ±45˚ plain-weave laminas over a 15.0 mm gauge section centered along the 170 mm model length to create the reduced thickness region for the monolithic hinge; this design supports an allowable fiber strain at 1.86%. This alteration reduces the element performance index for bending loading by 15%, from 1,187 to 1,014. Although maintaining the 178 μm thick gauge section and embedding two 305 μm thick by 1.47 mm wide NiTi wires 45.0 mm long within the uni-directional laminas along the outside edges of the tape-spring, centered over the reduced thickness region, reduces the index by 9%, from 1,187 to 1,077, compared to the axially, prismatic model; recall the thicker wires can accommodate the same radius as the CRFP through superelastic deformation. High temperature phase or austenite NiTi properties were assumed at E=75.0 GPa and ν=0.3.[9] This reinforcement is partly the enhancement the SMA flexure features purchase DECSMAR.

An additional dimension of the design space, temperature, exists attributable to the thermal-mechanical coupling of Nitinol's properties. For one engineering an SMA reinforced structure, several relevant issues must parallel the mechanics design to insure successful leverage of these features. Near eutectic NiTi micro-structure can only recover from detwinning, deformation mechanism enabling inelastic strain limits measured between 8-9%;[10, 11] if the crystal lattice responds through twin boundary deformation along the martensite plane as a body centered tetrahedral, a less symmetric atomic ordering indicative of the low temperature phase or martensite.[12, 13] Thermoelastic phase transformation from the more ordered austenitic face centered cubic (FCC) micro-structure can

be induced by an enthalpy rejection, motivation for the phenomenon commonly referred to as the shape memory effect (SME), a mechanical energy addition, or a combination of the two phenomena; tensile strain resulting from tractions and body loads also affects the transformation kinetics as a mechanical energy addition will result in stress induced martensite to a ceiling of approximately 50-80 K above the austenite finish temperature.[14] The engineering challenge is to spec an alloy which will be austenitic in the deployed service environment to exploit the higher performance FCC properties, but will not revert to austenite when subjected to integration and launch thermal-mechanical loads; if FCC retransformation occurs once strain packaged the detwinning deviatoric mechanism may be exhausted and the SMA will respond to loads above the austenite proportional limit by slip or conventional plastic deformation. As a logistics example, the particular Nitinol alloy used for proto-typing has austenite finish and martensite start temperatures at approximately 260 K and 220 K, respectively. Once stowed, plastic deformation can be avoided by not exceeding 310-340 K and once deployed austenite properties can be expected by not ceding 220 K; to maximize deployment force margain, events should transpire above austenite finish so as not to rely on the SME to utilize the detwinning strain energy.

Prototyping efforts approximated the reference design with the same radius and subtended angle, but with a laminate composed of two 200 µm cured thickness ±45° plain-weave IM7/977-2 laminas. In order to appreciate the compromise of effective section modulus incurred by deviating from the reference layup scenario, a hinge element constructed of the prototype sequence was modeled and evaluated. With only two plys a symmetric hinge through the thickness is unreasonable. The asymmetric prototype hinge is formed by removing one ±45° plain-weave lamina over a 15.0 mm gauge section centered along the 170 mm model length to create the reduced thickness region and embedding two 305 µm thick by 1.47 mm wide NiTi wires 45.0 mm long anchored within the plain-weave laminas along the outside edges of the tape-spring, centered over the reduced thickness region (Fig. 8); this design supports an allowable fiber strain at 1.48% and SMA strain at 8.48% assuming the NiTi wires have no authority on the neutral plane. This SMA strain magnitude toes the as mentioned recoverable inelastic strain limit for the alloy; some conventional plastic deformation may occur upon packaging the proto-type in addition to the detwinning depending upon neutral plane shift. The axial buckling prediction for the prototype hinged tape-spring is illustrative of the non-Euler column buckling modes germane to local failure of DECSMAR systems; axial buckling first occurs at 870 N for this model (Fig. 9).

Fig. 8 Embedded 305 µm thick by 1.47 mm wide NiTi wire 45.0 mm long anchored within the plain-weave laminas along the outside edges of the tape-spring, centered over the reduced thickness region

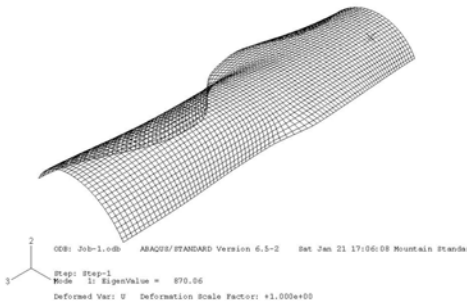

Fig. 9 Axial buckling prediction for the prototype hinged tape-spring is illustrative of the non-Euler column buckling modes germane to local failure of DECSMAR systems; axial buckling first occurs at 870 N for this model.

This critical load along with axial stiffness response and linear mass density distil to a longeron bending performance index of 842, 22% less than the more efficient hinged reference design. Initial observations indicated the NiTi wires enforced a more uniform radius transverseing across the folded hinge, mitigating stress concentration at the center and resulting in a more robust hinge. This as yet unquantified benefit is the balance of the enhancement the SMA flexure features purchase DECSMAR.

III. Point Design of an 180 mm Radius DECSMAR Boom

A. Design

The prototype approximation of the reference CFRP tape-spring element was extrapolated to a truss network. Batten frequency or truss radius was driven by bay length and a design goal of diagonal angle at 30˚ is a compromise between bending and column loading.[8] Bay length is the span of the element studied and an additional hinge; recall longerons z-fold, therefore two hinges are required per bay. Consequently, 185 mm bays and a 30˚ diagonal angle determine 262 mm length battens and 180 mm three-longeron truss cross-section radius. A 2.69 m, 14-bay DECSMAR variant, including a mid-board bulkhead, is depicted as a solid model and prototyped (Fig. 10).

(a) **(b)**

Fig. 10 185 mm bays and a 30˚ diagonal angle determine 262 mm length battens and 180 mm three-longeron truss cross-section radius. A 2.69 m, 14-bay DECSMAR variant, including a mid-length bulkhead, is depicted as a, (a) solid model; (b) and prototyped.

Once the bay geometry was resolved, the design methodology proceeded to consideration of the batten elements. Battens serve strength functions in both torsion and shear loading of a trussed boom. Murphey[8] presents the relations between individual longeron, diagonal, and batten member Euler buckling loads to global loading of the structure. If, for example, the most demanding loading scenario for the proto-typed boom was expected to arise from angular acceleration upon slewing, the greatest manageable moment can be solved based on the critical load of the longeron. Again, the first negative pivot of the proto-typed CFRP tape-spring hinged element occurs at 870 N, but the true repetitive longeron element found in the truss is an additional hinge longer; this recurring element extends from the center of a hinge through a second hinge and terminates at the center of the third, for a total length of 0.185 mm. The first negative pivot of this element occurred at 822 N; as a reference, the same finite element model less the NiTi reinforcement buckles at 551 N. Employing Eq. 2 the greatest manageable moment is 222 Nm.

$$P_l = \frac{2M}{nR} \text{ (Ref. 8)} \tag{2}$$

The global shear load can be estimated by dividing this result by the moment arm. To ensure the design is suitable in either the 14 bay, as depicted in Fig. 10, or seven bay, by removing the mid-length bulkhead and outboard seven bays, configurations for the loading scenario, the severest moment arm for shear loading, the length of the seven bay configuration, was assumed at a shear load of 171 N. Employing Eq. 3, from this shear load the required critical load of the batten can be inferred at 114 N.

$$P_b = 2\frac{V}{n} \text{ (Ref. 8)} \tag{3}$$

Longerons with a subtended angle at 120˚ lend well to three-longeron trusses as the battens interface tangentially, but without any benefit of limiting the batten angle, 180˚ was subtended for increased performance as eluded in Fig. 10. It was early apparent the batten cross-section would need to be modified from prismatic to yield a packaged geometry with the ability to nest; a batten design, characterized by the 400 μm thick plain-weave prototype laminate, subtending an angle of 180˚, and a radius of 19.1 mm, was selected and numerically forecast, in a similar manner to the study of the CFRP tape-spring element, to have a first negative pivot at 1.23 kN. This margin could be expended to qualify a non-prismatic batten for the strength requirements. In this way, the batten design was tailored to a strength-stability requirement traced along a critical design path originating from a global loading scenario.

The complication of nesting the prismatic batten is illustrated by Fig. 11a; the drawn angle on the packaged batten must be greater than 90˚ if the battens of the subsequent bay are expected nest. Recall the prototyped longeron hinge fiber strain design is 1.48%, translating to a radius of 4.77 mm; bay packaged length is equivalent to a z-fold or one hinge diameter, consequently like points of battens stand-off by this same axial distance once stowed. Since this stand-off is greater than the arc-length of the batten cross-section, battens must have the ability to nest in order to realize the longeron strain limited bay packaged length. A design was iterated to through virtual prototyping, modifying and analyzing concepts with 3D modeling and ABAQUS tools, which accommodates the aforementioned kinematics (Fig. 11b). This series of quadratic cross-section transitions stows to a drawn angle of 96˚ and is notable as the bending neutral planes of the cross-sections are coaxial to avoid inherent eccentricity (Fig. 11c). The critical load of this batten was numerically predicted at 671 N, expending some of the provided margin.

(a) **(b)** **(c)**

Fig. 11 (a) The drawn angle on the packaged batten must be greater than 90˚ if the battens of the subsequent bay are expected nest; (b) This design was iterated to through virtual prototyping which accommodates the aforementioned kinematics; (c) Series of quadratic cross-section transitions stows to a drawn angle of 96˚.

The third truss element of this DECSMAR boom variant, diagonals, although not prototyped, were considered to complete the system design. It was anticipated these members will be tension only elements to comply with the kinematics; design was driven by only their stiffness functions. Often in practice diagonals are sized to limit cantilever deflection attributable to shear compliance within a proportion of the effective stiffness including bending mechanisms. As an exercise, to limit cantilever shear compliance to 10%, based on mechanics of materials assumptions,

$$GA \geq \frac{27EI}{L^2}, \tag{4}$$

where Murphey[8] has proposed,

$$EI = \frac{n}{2}(EA)_l R^2, \tag{5}$$

and,

$$GA = \frac{n}{2}\frac{(EA)_l (EA)_d \cos^2\theta \sin\theta}{(EA)_l + (EA)_d \sin^3\theta}. \tag{6}$$

As the cross-section axial modulus of the 185 mm length repetitive longeron element with NiTi reinforced hinges was numerically forecast at 454 kN, the like property of the diagonal must be at least 764 kN, again relative to a seven-bay configuration. This role is suited by a bundle of dozen 12k IM7 fiber tows. If the designer determines this element is paced by torsion loading, the diagonals can be sized to match the torsion frequency to the first bending mode. To be conservative, the structural linear mass of the point design 14 bay truss network was assumed to reside along an annulus with the same radius as the cross-section, 180 mm, at the free end of the structure and a point mass at four times the structural mass was included at this same location located on the truss's axis, thus not contributing to the polar inertia. For this 20% structural mass fraction scenario torsional rigidity relates to bending rigidity by,

$$GJ = \frac{9EIR^2}{35L^2}, \tag{7}$$

to match the respective modes' frequencies, where Murphey[8] has proposed,

$$GJ = \frac{R^2 n \cos^2\left(\frac{\pi}{n}\right)(EA)_l (EA)_d \cos\theta}{(EA)_l \cot\theta + \left((EA)_l + (EA)_d \sin\theta\right)\tan\theta}. \tag{8}$$

The diagonal cross-section modulus must be 3.04 kN, now relative to a 14 bay configuration. This role is suited by less than a single bundle of 6k IM7 fiber tows.

B. Experiment

The proto-typed structure was strain instrumented and progressively loaded with a transverse force applied at the free-end, acting parallel and opposite sense to gravity. Correlation of the measured strain fields was sought to a numerical model representing the truss; this model included the features of the SMA reinforced hinges and accounted for body loading due to gravity. A representative comparison is the longitudinal strain of the top longeron at bay 12 as numbered from the fixed-end (Fig. 12). The model was expected to respond with greater stiffness as the battens were assumed bonded to the longerons where as this interface was proto-typed with mechanical fasteners permitting some compliance.

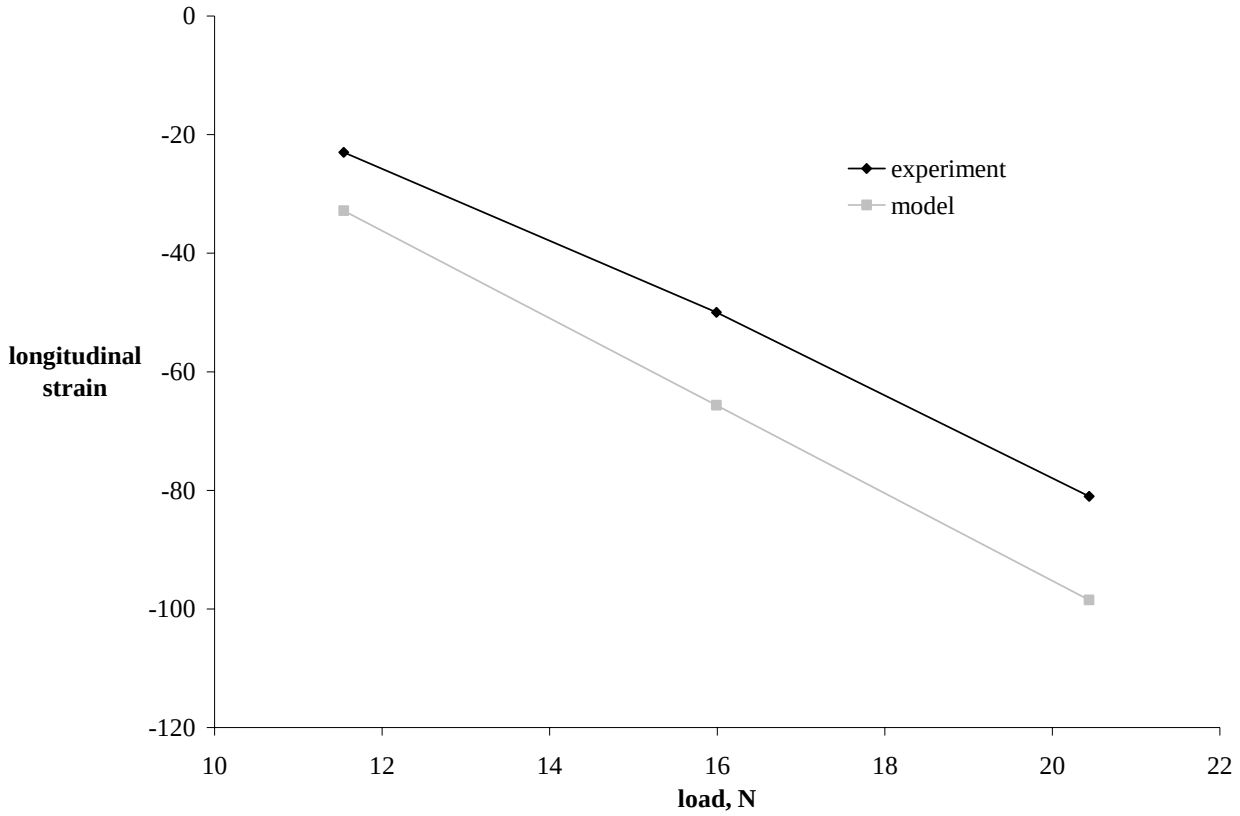

Fig. 12 Representative comparison is the longitudinal strain of the top longeron at bay 12 as numbered from the fixed-end.

This agreement lends credibility to the fidelity of the numerical model and thus it's utility for capturing the load-path allocation between the frame-like longerons and battens. Moment communication through the latter elements was quantified by determining the maximum moment attributable to the 20.4 N loading scenario in a bay 12 batten communicating between the top and one of the bottom longerons; the longitudinal strain field is contoured (Fig. 13). This moment, resulting from shear loading boundary conditions at the longeron interfaces is three-orders of magnitude less than the global moment, yet considering this equivalent magnitude is developed in the other 27 battens resisting shear between the top and two-bottom longerons, the total moment reacted in the batten elements is one-order of magnitude less than the global; this allocation is a significant departure from a true truss-like response. This observation portends depth strength-stability scaling phenomena unique to a monolithic truss with the ability to proportion energy imparted from global loading to complex stress states through the structural network.

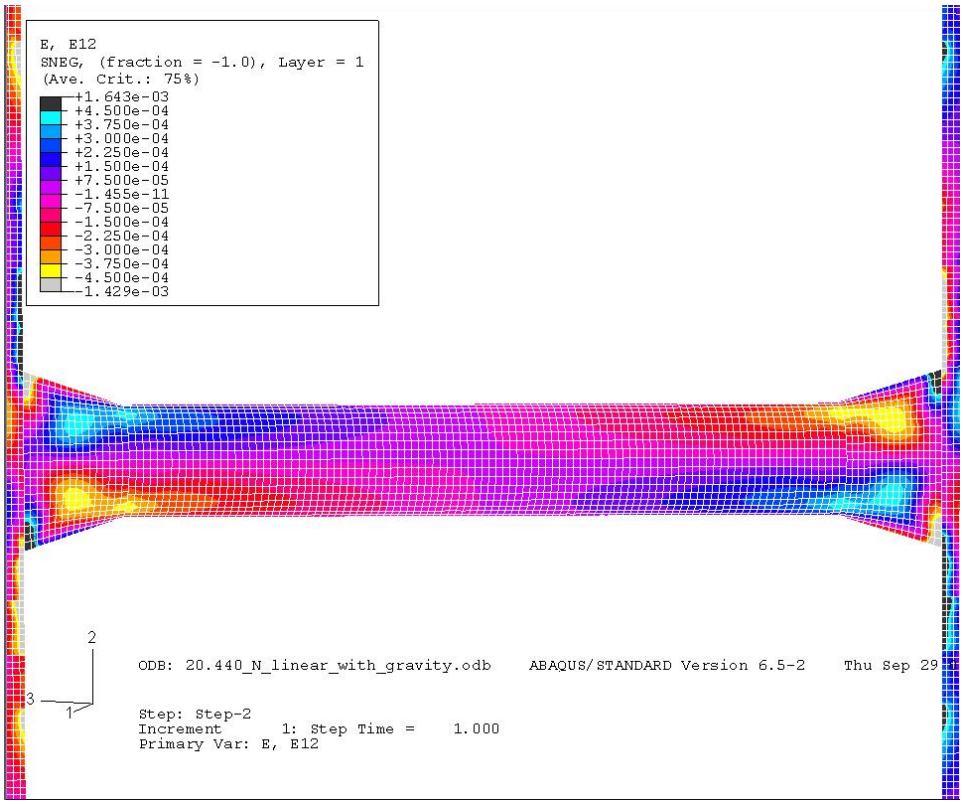

Fig. 13 Moment communication through the latter elements was quantified by determining the maximum moment attributable to the 20.4 N loading scenario in a bay 12 batten communicating between the top and one of the bottom longerons; the longitudinal strain field is contoured.

IV. Performance Implications of Scaling the Truss Radius

A numerical study of bay-scale DECSMAR elastic-stability and stiffness properties has been conducted for parametrically varying radius of gyration; influence of the SMA reinforced hinge sections and linear compaction ratio were tracked as additional performance implications of scaling the truss depth. Finite element forecasts were performed with the same modeling parameters as the study of the CFRP tape-spring element. Figure 14 depicts the trades in strength, represented by linear specific critical moment,

$$M_{ls} = \frac{M}{w}, \tag{9}$$

and stiffness, represented by linear specific bending modulus,

$$(EI)_{ls} = \frac{EI}{w}, \tag{10}$$

of increasing radius finite element models composed of prismatic elements with identical non-hinged longeron and batten cross-section radius and subtended angle to the point design, but with the reference laminate; batten frequency is comparable and, again, diagonals were not incorporated. As the cross-sections were controls, members slender with greater truss radius. Note in general, stiffness is traded for strength with increasing depth, but a competing trend dominates DECSMAR trusses as they exhibit frame-like behavior; moment communication among members leads to a susceptibility to coupled bending modes at smaller radii.

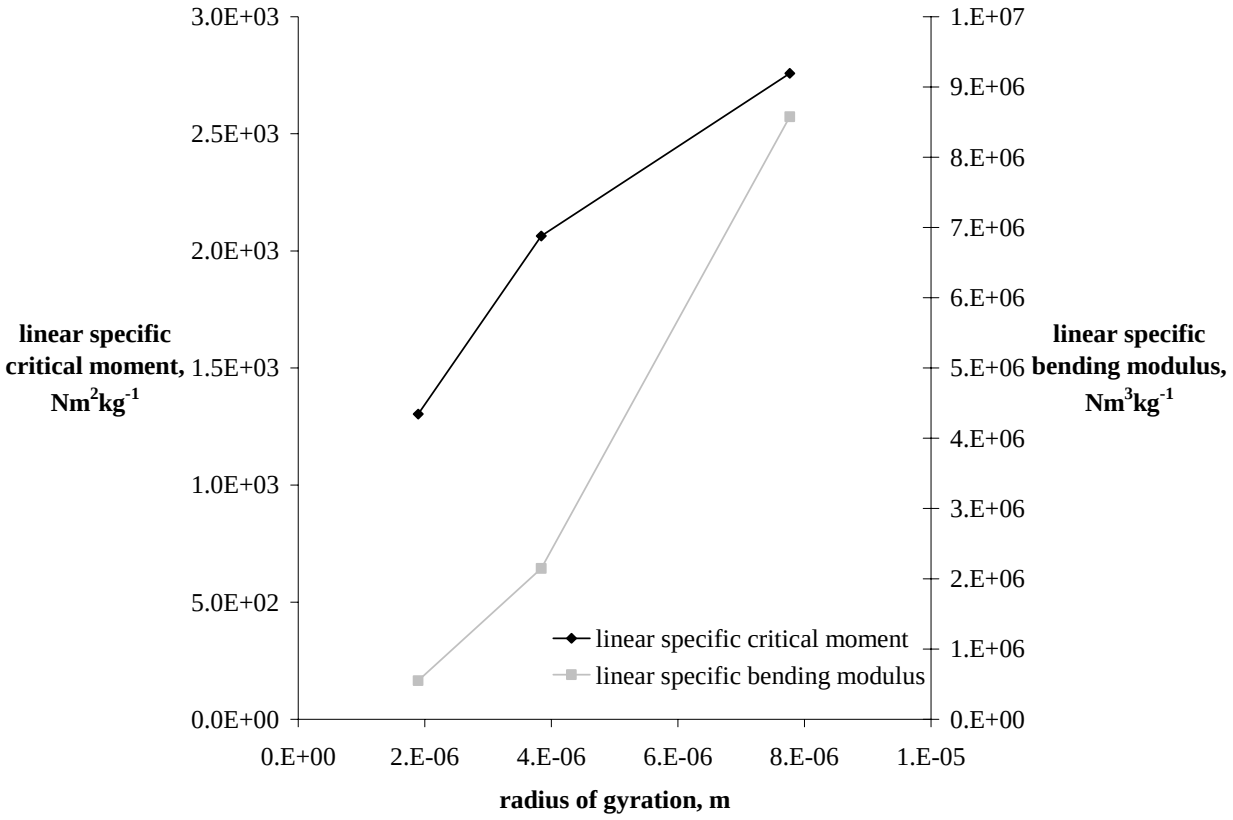

Fig. 14 Trades in strength, represented by linear specific critical moment, and stiffness, represented by linear specific bending modulus, of increasing radius finite element models composed of prismatic elements with identical non-hinged longeron and batten cross-section radius and subtended angle to the point design, but with the reference laminate; batten frequency is comparable and, again, diagonals were not incorporated.

To appreciate the enhancement the SMA flexure features purchase DECSMAR at the system level, a design exercise was entertained traceable to radar systems. A 475 m, one-dimensional platform with passive stability critical design requirements of 100 μrads^{-2} angular acceleration, processing about mid-length, and 0.020 Hz first free-free mode managed with 20% structural mass fraction was sought;[15] discounting shear compliance, the pairing of linear specific critical moment at 2.51 kNm^{2}kg^{-1} and linear specific bending modulus at 8.03 MNm^{3}kg^{-1} will satisfy the strength and stiffness requirements, respectively. Of the set evaluated for Fig. 14, the model identified by a radius of gyration value of 7.77 μm qualifies at 2.76 kNm^{2}kg^{-1} and 8.58 MNm^{3}kg^{-1}. This 720 mm radius, triple the point design, DECSMAR variant has a structural linear mass of 178 gm^{-1}, moment strength-stability at 490 Nm, bending modulus at 1.52 MNm^2, and 1.34% compaction ratio; this packaging efficiency was found assuming the same allowable fiber strain for the ±45˚ plain-weave laminas as the 0˚ uni material of the hinged variation of the reference longeron, 1.86%. One could expect to lose 37% moment strength-stability and 1% bending modulus, yet gain 0.01% compaction ratio by removing the ±45˚ plain-weave laminas over the 15.0 mm gauge sections to incorporate the monolithic hinge features, discounting mass deltas attendant to this alteration (Table 2).

Table 2 Enhancement the SMA flexure features purchase DECSMAR at the system level

Configuration	Linear Mass, gm^{-1}	Critical Moment, Nm	Bending Modulus, MNm^2	Compaction Ratio, %
R=720 mm	178	490	1.52	1.34
R=720 mm (hinged)	~178	309	1.50	1.33
R=720 mm (SMA reinforced hinged)	~178	456	1.52	1.33

Performance loss from the prismatic model was based on the reduction in Euler column buckling load and axial modulus of the reference CFRP tape-spring element as these properties have been shown proportional to truss moment strength-stability per Eq. 2 and bending modulus per Eq. 5, respectively.[8] Among the performance metrics stipulated for this design scenario, the hinged truss would not satisfy the strength requirement as it can tolerate accelerations to 69.1 $\mu rads^{-2}$. Embedding the identical NiTi additions within the reduced thickness region results in a reduction of elastic-stability by 7% from the prismatic model; accelerations to 102 $\mu rads^{-2}$ are manageable, again discounting mass deltas attendant to this alteration. The SMA flexures effectively serve a strength function for this exercise; this dividend as well as previously discussed packaging robustness and increased strain energy capacity to motivate self-deployment may be mission enabling pending design requirements. The designer must be aware of slenderness issues to appreciate discrepancies between theoretical and actual performance when scaling for greater structural depth; Refs. 8 and 16 offer valuable discussions on this subject.

V. Conclusion

In review, research to develop a novel self-deployable truss architecture composed of CFRP tape-spring elements and embedded SMA flexures has been documented; this particular structural system is referred to as DECSMAR and is representative of a concentrated, material deformation based deployable architecture. First, the design space of the individual CFRP tape-spring element was defined. The higher qualifying laminate candidate, considered a reference for the remainder of the manuscript, was composed of 30% $\pm 45^{\circ}$ off-axis fiber proportion to serve a strength function to the balance of sandwiched 0° material. Strength can be gained through greater laminate thickness at subtended angles to approximately 50°, beyond, diminishing geometric stiffness dominates; although, another trend must be considered. For a particular allowable fiber strain, hinge radius and compaction ratio increase proportionally with laminate thickness. Qualitatively, optimal CFRP tape-spring element designs can subtend angles up to 80° based on the trends presented representing a fixed linear mass. Finite element predictions suggests increased performance can be achieved by decreasing radius and increasing subtended angle, but cross-sections greater than 180° may not be reasonable to serve kinematically as a monolithic hinge. Features of the hinge were incorporated into the reference model by removing the $\pm 45^{\circ}$ plain-weave laminas over a gauge section centered along the model length to create the reduced thickness region for the monolithic hinge; this alteration reduces the element performance index for bending loading by 15%. Although maintaining the gauge section and embedding two NiTi wires within the uni-directional laminas along the outside edges of the tape-spring, centered over the reduced thickness region, reduces the index by 9%; this reinforcement is partly the enhancement the SMA flexure features purchase DECSMAR.

An additional dimension of the design space, temperature, exists attributable to the thermal-mechanical coupling of Nitinol's properties. The engineering challenge is to spec an alloy which will be austenitic in the deployed service environment to exploit the higher performance FCC properties, but will not revert to austenite when subjected to integration and launch thermal-mechanical loads; if FCC retransformation occurs once strain packaged the detwinning deviatoric mechanism may be exhausted and the SMA will respond to loads above the austenite proportional limit by slip or conventional plastic deformation.

An exercise for a point design of a 180 mm radius DECSMAR boom with correlation to experimental analysis was conducted. Bay geometry was resolved driven by the CFRP tape-spring element length and a design goal of diagonal angle at 30°. The methodology proceeded to consideration of batten elements; the design of these members was based on the strength function they serve in shear loading to realize the manageable moment of the truss solved from the strength-stability of the longerons. A margin was included as it was early apparent the batten cross-section would need to be modified from prismatic to yield a packaged geometry with the ability to nest. In this way, the batten design was tailored to a strength-stability requirement traced along a critical design path originating from a global loading scenario. A non-prismatic design was iterated to exhibiting a series of quadratic cross-section

transitions accommodating the strain limited stowed state. The third truss element of this DECSMAR boom variant, diagonals, although not prototyped, were considered to complete the system design; these elements were sized both to limit cantilever shear compliance to 10% and, if the designer determines this element is paced by torsion loading, to match the torsion frequency to the first bending mode.

The proto-typed structure was strain instrumented and progressively loaded with a transverse force applied at the free-end, acting parallel and opposite sense to gravity. Correlation of the measured strain fields was sought to a numerical model representing the truss. The total moment reacted in the batten elements is one-order of magnitude less than the global; this allocation is a significant departure from a true truss-like response. This observation portends depth strength-stability scaling phenomena unique to a monolithic truss with the ability to proportion energy imparted from global loading to complex stress states through the structural network.

Finally, performance implications of scaling the truss radius were explored. Note in general, stiffness is traded for strength with increasing depth, but a competing trend dominates DECSMAR trusses as they exhibit frame-like behavior; moment communication among members leads to a susceptibility to coupled bending modes at smaller radii. The SMA flexures effectively serve a strength function for this exercise; this dividend as well as previously discussed packaging robustness and increased strain energy capacity to motivate self-deployment may be mission enabling pending design requirements. The designer must be aware of slenderness issues to appreciate discrepancies between theoretical and actual performance when scaling for greater structural depth.

Fundamental principles of rational boom design relevant to all deployable structures have been applied to the DECSMAR architecture. Technology addressed through this research is intended to foster and mature successive large, launch-packaged concentrated strain structures.

Acknowledgments

Support of this research is provided by the Air Force Research Laboratory Space Vehicles Directorate monitored by Dr. Jeffry S Welsh.

References

[1]Jones, RM, *Mechanics of Composite Materials: 2nd Edition*, Brunner-Routledge, New York, NY, 1999.

[2]Yee, JCH, Soykasap, O, & Pellegrino, S, "Carbon Fiber Reinforced Plastic Tape Springs," *Proceedings of the 45th AIAA/ASME/ASCE/AHS/ASC Structures, Structural Dynamics, and Materials Conference*, 2004-1819, AIAA, Washington, DC, 2004.

[3]Birman, V, "Review of Mechanics of Shape Memory Alloy Structures," *Applied Mechanics Reviews*, Vol. 50, 1997, pp. 629-645.

[4]*Deployable Structures*, Edited by S Pellegrino, CISM Courses & Lectures, CISM, 2001.

[5]*ABAQUS/Standard User's Manual*, Hibbitt, Karlsson, & Sorensen, Inc., 2005.

[6]Timoshenko, S, & Gere, J, *Theory of Elastic Stability: 2nd Edition*, McGraw-Hill, New York, NY, 1961.

[7]Welsh, JS & Wegner, PM, "The Effect of Adhesive Bond Thickness and Material Type on Structure Stiffness," *Proceedings of the 43rd AIAA/ASME/ASCE/AHS/ASC Structures, Structural Dynamics, and Materials Conference*, 2002-1726, AIAA, Washington, DC, 2002.

[8]*Recent Advances in Gossamer Spacecraft*, Edited by CHM Jenkins, Progress in Astronautics & Aeronautics, AIAA, Washington, DC, 2006.

[9]Hodgson, DE, Wu, MH, & Biermann, RJ, "Shape Memory Alloys," Johnson Matthey, 2004.

[10]Cross, WB, Kariotis, AH, & Stimler, FJ, "Nitinol Characterization Study," NASA CR-1433, 1970.

[11]Proft, JL & Duerig, TW, "Mechanical Aspects of Constrained Recovery." *Engineering Aspects of Shape Memory Alloys*, Edited by TW Duerig, KN Melton, D Stockel, & CM Wayman, Butterworth-Heinemann, London, UK, 1990, pp. 115-129.

[12]Tanaka, K, "Analysis of Recovery Stress and Cyclic Deformation in Shape Memory Alloys," *Advances in Continuum Mechanics*, Edited by O Bruller, Springer-Verlag, Berlin, D, 1991, pp. 441-451.

[13]Funakubo, H, *Shape Memory Alloys*, Gordon and Bleach, New York, NY, 1987.

[14]Xu, YB, Wang, RL, & Wang, ZG, "In-Situ Investigation of Stress-Induced Martensite Transformation in the Ni-Ti Shape Memory Alloy During Deformation," *Material Letters*, Vol. 24, 1995, pp. 355-358.

[15]Blevins, RD, *Formulas for Natural Frequency and Mode Shape*, Van Nostrand Reinhold Company, 1979.

[16]Hedgepeth, JM, "Critical Requirements for the Design of Large Space Structures," NASA CR-3484, 1981.